Title

High-resolution in vivo diffusion tensor imaging of the injured cat spinal cord using self-navigated, interleaved, variable-density spiral acquisition (SNAILS-DTI)

Journal

Magnetic Resonance Imaging, 28(9)

ISSN

0730-725X

Authors

Ellingson, Benjamin M
Sulaiman, Olawale
Kurpad, Shekar N

Publication Date

2010-11-01

DOI

10.1016/j.mri.2010.06.006

Peer reviewed

Available online at www.sciencedirect.com
ScienceDirect
Magnetic Resonance Imaging 28 (2010) 1353–1360
MAGNETIC RESONANCE IMAGING

High-resolution in vivo diffusion tensor imaging of the injured cat spinal cord using self-navigated, interleaved, variable-density spiral acquisition (SNAILS-DTI)

Benjamin M. Ellingson[a,c], Olawale Sulaiman[b], Shekar N. Kurpad[c,*]

[a]*Department of Radiological Sciences, David Geffen School of Medicine at UCLA, Los Angeles, CA 90095, USA*
[b]*Department of Neurosurgery, Ochsner Clinic Foundation, New Orleans, LA 70121, USA*
[c]*Department of Neurosurgery Medical College of Wisconsin, Milwaukee, WI 53226, USA*

Received 8 December 2009; revised 12 January 2010; accepted 10 June 2010

Abstract

Diffusion tensor magnetic resonance imaging (DTI) is useful for studying the microstructural changes in the spinal cord following traumatic injury; however, image quality is generally poor due to the small size of the spinal cord, physiological motion and susceptibility artifacts. Self-navigated, interleaved, variable-density spiral diffusion tensor imaging (SNAILS-DTI) is a distinctive pulse sequence that bypasses many of the challenges associated with DTI of the spinal cord, particularly if imaging gradient hardware is of conventional quality. In the current study, we have demonstrated the feasibility of implementing SNAILS-DTI on a clinical 3.0-T MR scanner and examined the effect of navigator filter parameters on image quality and reconstruction time. Results demonstrate high-quality, high-resolution (546 μm×546 μm) in vivo DTI images of the cat spinal cord after traumatic spinal cord injury.
Published by Elsevier Inc.

Keywords: DTI; Diffusion tensor imaging; Spiral MRI; SNAILS; Spinal cord injury; Cat; SCI

1. Introduction

Diffusion tensor imaging (DTI) of the spinal cord is particularly challenging due to magnetic susceptibility-related T_2* signal attenuation and distortion from the bony vertebral column, chemical-shift artifacts from epidural fat, spinal cord motion associated with cerebrospinal fluid (CSF) pulsations and the relatively small size of the cord relative to the excited tissue volume. Diffusion imaging using MR is inherently sensitive to motion and changes in susceptibility that causes signal attenuation and poor estimates of apparent diffusion coefficients (ADCs). Motion of the spinal cord caused by pulsating CSF can cause ghosting in the T_2-weighted and diffusion-weighted images, which can further affect ADC estimates. These challenges have led to the development of novel pulse sequences including line scan diffusion imaging [1–3], readout-segmented echoplanar imaging (EPI) [4], navigator-segmented EPI [5], ZOOM-EPI [6] and BLADE (PROPELLER)-DTI [7].

Self-navigated interleaved spiral DTI (SNAILS-DTI) [8] is a distinctive pulse sequence that bypasses many of the challenges associated with DTI of the spinal cord, particularly if imaging gradients are of conventional quality (not high performance). For example, phase distortions from T_2* or susceptibility effects are naturally reduced because spiral acquisition does not require phase encoding. The efficient coverage of *k*-space using spiral acquisition can allow for shorter echo times (TEs) to be employed, which further reduces the effects of T_2* decay. Since the outer edges of *k*-space are typically not collected, shorter acquisition times can be employed for a given amplitude and/or slew rate limit. Multishot spiral acquisition schemes allow self-navigation and moment-nulling motion compensation [9], which may be particularly useful for suppressing effects of spinal cord motion during CSF pulsation. Lastly, variable-density spiral designs [10] allow for oversampling of central *k*-space, which can further reduce motion-related

* Corresponding author. Tel.: +1 414 805 5434.
E-mail address: skurpad@mcw.edu (S.N. Kurpad).

0730-725X/$ – see front matter. Published by Elsevier Inc.
doi:10.1016/j.mri.2010.06.006

signal attenuation and allow for higher spatial resolution with minimal geometric distortion. We hypothesized that the inherent properties of the self-navigating, interleaved, multishot, variable-density spiral DTI sequence may be particularly beneficial for obtaining low-cost, high-resolution diffusion images of the spinal cord in preclinical animal models using clinically available MR systems and conventional gradient hardware.

In the current study, we have implemented a self-navigating, interleaved, multishot, variable-density spiral DTI (SNAILS-DTI) sequence specific to a clinical 3.0-T MR scanner and gradient hardware set to obtain diffusion anisotropy measurements before and after traumatic spinal cord injury (SCI) in a cat model. To test the utility of SNAILS-DTI, we first qualitatively compare differences in image quality between echoplanar (EPI) and variable-density spiral acquisitions to illustrate the advantages of SNAILS acquisition over EPI on conventional MR systems. Then, we examine the effects of the navigator filter design on signal-to-noise ratio (SNR), diffusion anisotropy measurements and eigenvector variability. Using the most favorable reconstruction parameters based on a reasonable trade-off between image quality and reconstruction time, we then compare in vivo measurements of fractional anisotropy (FA) within the neurologically intact and traumatically injured cat spinal cord at a spatial resolution higher than those previously reported in vivo [11].

2. Methods

2.1. MRI

All in vivo DTI images were prescribed in real time using a clinical long-bore 3.0-T MR scanner (GE Signa Excite; GE Medical Systems, Milwaukee, WI) with maximum gradient strength g_m=40 mT/m and maximum slew rate s_m=150 mT/m/s. A quadrature knee coil was used for radiofrequency transmission and reception. The *k*-space trajectory for variable-density spiral acquisition presented by Kim et al. [10] was employed according to the equation:

$$k(\tau) = \lambda \tau^{\alpha} e^{j\omega\tau} \quad (1)$$

where τ=[0,1], $\omega=2\pi n$, n is the number of turns in *k*-space, λ is a constant equal to N/[2×field of view (FOV)], N is the desired matrix size and α is a parameter that determines the amount of oversampling (i.e., spiral pitch factor) in either central *k*-space (α>1) or at high *k*-space values (α<1). Note that this form is analogous to the design work by Glover [12] for conventional spiral acquisition. The pulse sequence for a single interleaf obtained from an oscilloscope trace with the variable-density pitch factor (α) set to 4 is illustrated in Fig. 1A and the resulting estimated *k*-space trajectory is illustrated in Fig. 1B. The pitch factor α=4 was chosen as a compromise between *k*-space coverage and acquisition time.

2.2. Animals

A total of five adult female, ovariectomized cats weighing 3–5 kg were used in this pilot study. Animals were divided into two groups: those who underwent a laminectomy without contusive injury (sham group; n=2; N1 and N2) and those who underwent a laminectomy with contusive injury (injury group; n=3; SCI1, SCI2 and SCI3).

2.2.1. Spinal cord injury

All animals underwent a surgical procedure (sham or injury) while under general anesthesia (Nembutal, 25 mg/kg). Animals were intubated, connected to a respirator and secured to an operating table in the prone position. Using sterile techniques, a laminectomy was performed on all animals at T8–9 levels to expose the dura and spinal cord. Contusive SCI was induced in animals in the injured group by dropping a small 25-g weight directly onto the spinal cord from a height of 12 cm (a 300-g-cm weight-drop event) using a linearly guided, computer-monitored weight-drop system that allowed simultaneous collection of data related to the mechanics of the weight-drop event [13]. The surgical site was irrigated with sterile saline and sutured in layers. Postoperative care of the animals included bladder expression until spontaneous voiding reflexes returned, plus administration of analgesics (Bupernex, 0.01 mg/kg), food supplements, antibiotics and lactated Ringer's solution. This procedure has been shown to result in immediate and profound hindlimb paralysis [13]. All surgical procedures were performed by a board-certified neurological surgeon (O.S.).

During the MRI procedures, all animals were anesthetized (ketamine, 30 mg/kg; atropine, 0.05 mg/kg sc one time in conjunction with thiopental 10–12 mg/kg iv to effect, approximately 2 h total). A non-injured, pre-surgical animal (N2) was scanned prior to any surgery for the purposes of pulse sequence optimization (comparison between EPI and SNAILS; optimization of Gaussian navigation filter for phase correction). This same animal was scanned again at 2, 4, 5 and 7 weeks after laminectomy. Another non-injured animal (N1) was scanned 4 and 5 weeks after laminectomy. Two of the animals with SCI (SCI1 and SCI2) were imaged 3, 4 and 5 weeks after contusion; however, due to technical issues, we were only able to obtain images of SCI3 at 3 and 5 days after contusion. The Animal Review Committees at the Medical College of Wisconsin and the Zablocki VA Medical Center, Milwaukee, WI, approved all protocols.

2.3. Echoplanar versus spiral acquisition

To compare image quality between the EPI and SNAILS acquisition schemes with a clinical MR system and conventional gradient hardware, we obtained images in a uniform water phantom and a single live, anesthetized, uninjured female cat (N2). Three-dimensional spoiled gradient echo (SPGR) images were acquired [TE/repetition time (TR)=1.8 ms/6.5 ms, resolution=546 μm×546 μm×1.5 mm]

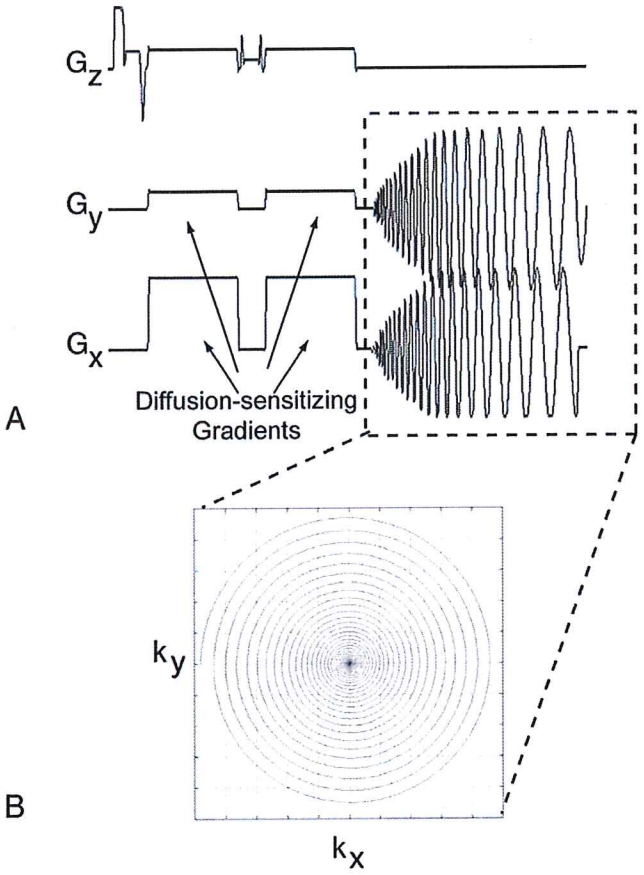

Fig. 1. Diffusion-weighted, variable-density, self-navigated interleaved spiral acquisition (SNAILS-DTI) pulse sequence and estimated *k*-space trajectory. (A) Pulse sequence obtained from the gradient waveforms acquired with an oscilloscope. Variable-density pitch factor was α=4. A single interleaf is shown. (B) Estimation of *k*-space trajectory from resulting gradient waveforms.

for visual comparison with EPI and SNAILS images. Axial DTI-EPI images were acquired with TE/TR=122.2 ms/17 s, matrix size=256×256, number of averages (NEX)=4, FOV=14 cm and slice thickness=3 mm with no interslice gap. For axial SNAILS-DTI images, TE/TR=55 ms/3 s, matrix size=256×256, FOV=14 cm, NEX=2, slice thickness=3 mm with no interslice gap, with 16 interleaves and a variable-density pitch factor (α)=4. Both DTI-EPI and SNAILS-DTI diffusion-weighted images were acquired with b=0 s/mm^2 and b=500 s/mm^2 in 25 directions; however, only the b=0 s/mm^2 images were used for comparison between acquisition techniques. The DTI-EPI utilized a twice-refocused spin-echo sequence [14] to reduce eddy current distortions forcing the DTI-EPI scans to have a substantially longer TE. Additionally, TR was also substantially longer in DTI-EPI compared with SNAILS-DTI to ensure maximum longitudinal magnetization for the next excitation. Both EPI-DTI and SNAILS-DTI images had comparable voxel sizes (546 μm×546 μm×3.0 mm). Note that the voxel size in the current study was smaller than those previously documented in vivo [11]. Raw MR data were phase corrected and reconstructed offline using custom MATLAB scripts, and the diffusion tensor was calculated using a nonlinear least-squares estimate also using offline custom MATLAB scripts.

2.4. Phase correction and image reconstruction

When using multiple interleaves with spiral acquisition, motion-induced phase correction must be performed on each interleaf prior to combining all interleaves in order to reduce the risk of spatially dependent signal cancellation. The iterative approach, outlined by Liu et al. [8], was used and implemented for phase correction and image reconstruction in the current study. Briefly, phase error was estimated by application of a Gaussian windowing function (navigator filter) around the center of *k*-space. After Fourier transformation, the low-resolution phase image was subtracted from the high-resolution, complex image. This process was then repeated multiple times until no significant change in the phase is observed from iteration to iteration. Additional details regarding the mathematics and processing steps are outlined by Liu et al. [8].

To find the most favorable size of the Gaussian navigator filter and most advantageous number of iterations of the phase correction algorithm, we examined (a) SNR [15], (b) the variance of the primary eigenvector of the diffusion tensor, (c) mean diffusivity and (d) FA in approximately 35 voxels in 10 slices (350 voxels total) within the spinal cord in a single uninjured cat (N2), while systematically changing the diameter of the navigator filter and iteration number. Specifically, we examined these imaging parameters as the diameter of the Gaussian window used as the navigator filter was varied from 5, 10, 15, 25, 50 and 100 voxels in diameter (corresponding to 0.36, 0.71, 1.07, 1.79, 3.57 and 7.14 cm^{-1}, respectively) and after 1, 2, 4 and 16 iterations through the phase-correction algorithm. Note that we chose to examine the variability in the primary eigenvector within the spinal cord because of the well-defined rostral–caudal orientation of spinal cord white matter tracts.

2.5. Comparison of injured to sham-injured spinal cords

After the pulse sequence and phase correction algorithm were tested, we compared FA estimates between injured and sham-injured animals. Twenty interleaved, contiguous axial images were collected, spanning 60 mm across the surgical site. Regions of interest were drawn around the entire spinal cord (i.e., no gray/white matter delineation) for each axial image using high-resolution SPGR images and T_2 images (b=0 s/mm^2). FA measurements were then plotted as a function of distance across the surgical site for all animals and all time points. Lastly, FA at the lesion site was compared with normal-appearing spinal cord distal from the lesion site and with FA measurements from sham-injured animals. To illustrate the differences between FA at the lesion site and in normal-appearing spinal cord, we averaged the FA values in the spinal cord across (a) three

contiguous slices at the lesion epicenter, (b) the first three contiguous slices (rostral) and (c) the last three contiguous slices (caudal) for all injured animals and all time points. We also compared these values to FA measurements averaged across the entire spinal cord in sham-injured animals. Because of low sample size, only qualitative observations were made.

3. Results

3.1. Echoplanar versus spiral acquisition

To determine whether or not image quality could be improved by using spiral acquisition, we imaged a uniform water phantom and an uninjured, anesthetized cat (N2) in vivo, both at a resolution of 546 μm×546 μm×3.0 mm. The results of these tests are summarized in Fig. 3. SPGR images of the uniform water phantom show relative homogeneity and little geometric distortions (Fig. 2A). Echoplanar acquisition of T_2 images (b=0 s/mm^2) showed significant ghosting artifact (Fig. 2B) and very low SNR (Fig. 2D). T_2 images (b=0 s/mm^2) acquired using SNAILS illustrated a high SNR (Fig. 2D) and a relatively homogeneous circular phantom (Fig. 2C). Phantom images acquired with SNAILS, however, did result in some geometric distortions near the edge of the images when compared with SPGR images (Fig. 2D).

SPGR images acquired in the live animal clearly illustrate the relatively small size of the spinal cord (Fig. 2E, arrow). Echoplanar T_2 images (b=0 s/mm^2) showed significant geometric distortion of the whole body, no discernable spinal cord anatomy and low SNR (Fig. 2F). T_2 images acquired using SNAILS illustrated excellent reproduction of spinal cord anatomy in the center of the image (Fig. 2F, arrow) with relatively high SNR. These results suggest that SNAILS acquisition with clinical MR systems and conventional gradient hardware are superior to EPI with respect to image quality and SNR.

3.2. Phase correction and image reconstruction

Estimates of SNR, primary eigenvector variance, mean diffusivity and FA for various navigator filter diameters and algorithm iterations are illustrated in Fig. 3. The SNR was highest for a single iteration and for a filter diameter of 10 voxels, or 0.71 cm^{-1} (Fig. 3A). The primary eigenvector variance (Fig. 3B), which should approach zero for the spinal cord because all axons are tightly packed and oriented in the same rostral–caudal direction, was around 12° for navigator filter sizes ranging from 5 to 10 voxels (0.36 to 0.71 cm^{-1}), regardless of the number of iterations. For navigator filter diameters larger than 10 voxels (0.71 cm^{-1}), the variance in the primary eigenvector direction decreased as the number of iterations increased, suggesting better estimates of the diffusion tensor for increasing filter diameter and number of iterations. Mean diffusivity within the uninjured spinal cord (Fig. 3C) was relatively low for a single iteration compared with multiple iterations. Mean diffusivity also appeared to decrease slightly for increasing filter diameters if more than a single iteration was employed. Estimates of FA also appeared different for a single iteration compared to measurements after multiple iterations (Fig. 3D).

We determined the best combination of reconstruction parameters based on a reasonable trade-off between image

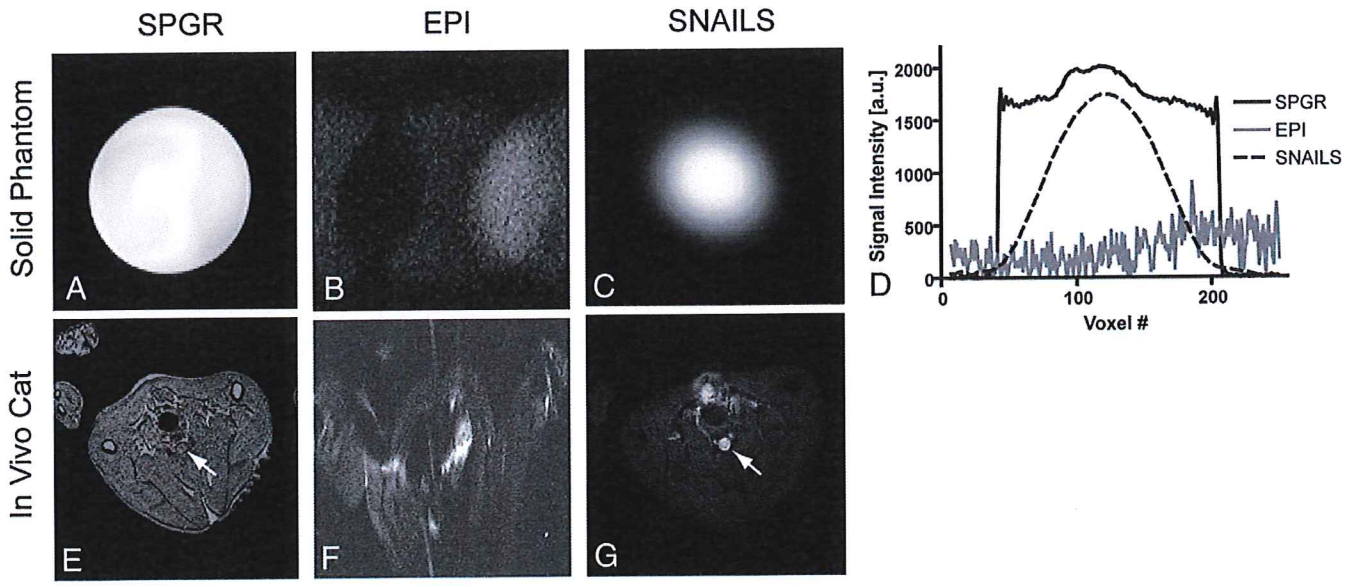

Fig. 2. SPGR, EPI and variable-density spiral acquisition (SNAILS) results for a uniform water phantom (top row) and uninjured cat (bottom row). (A) SPGR images, (B) EPI images and (C) SNAILS images for the uniform water phantom. (D) Horizontal line profiles through phantom images showing SPGR, EPI and SNAILS signal intensity differences. (E) SPGR images, (F) EPI images and (G) SNAILS images for an uninjured cat (N2).

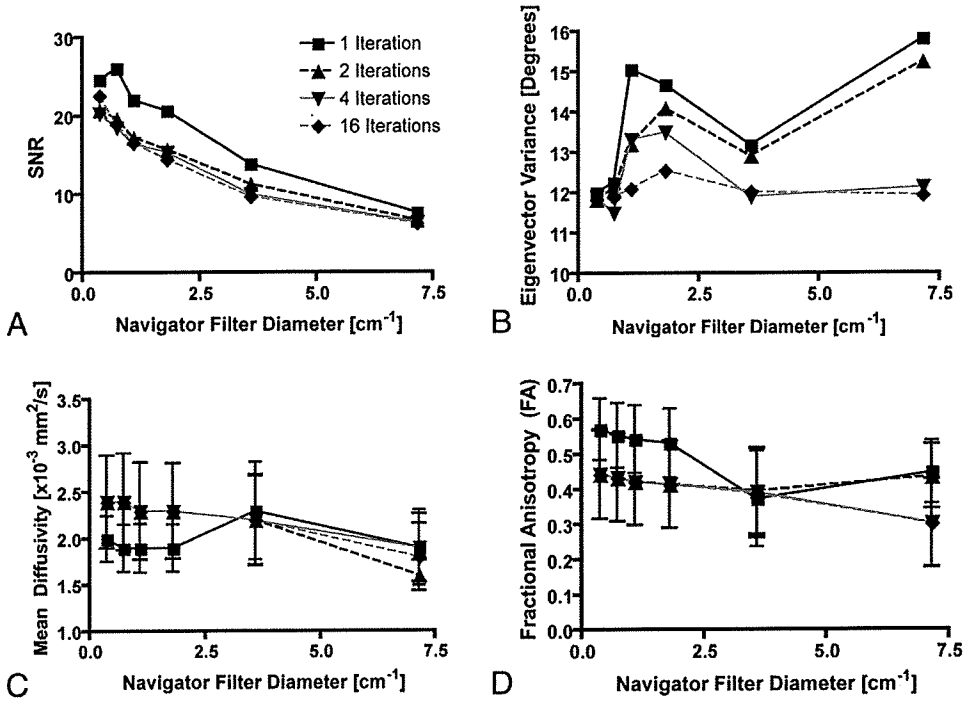

Fig. 3. Reconstruction parameters results. (A) SNR, (B) variance in primary eigenvector, (C) mean diffusivity and (D) FA for various Gaussian navigator filter diameters and number of iterations through the reconstruction algorithm.

quality and reconstruction time to be a navigator filter diameter of 10 voxels (0.71 cm^{-1}) and two iterations through the reconstruction algorithm. This combination of filter size and number of iterations will provide a relatively high SNR, low eigenvector variance and reasonable estimates of both mean diffusivity and FA while maintaining a relatively low computational time compared with a greater number of iterations. (Computational time increases linearly with the number of iterations.)

3.3. Comparison of injured to sham-injured spinal cords

In general, DTI using spiral acquisition (SNAILS-DTI) resulted in excellent image quality within the spinal cord and

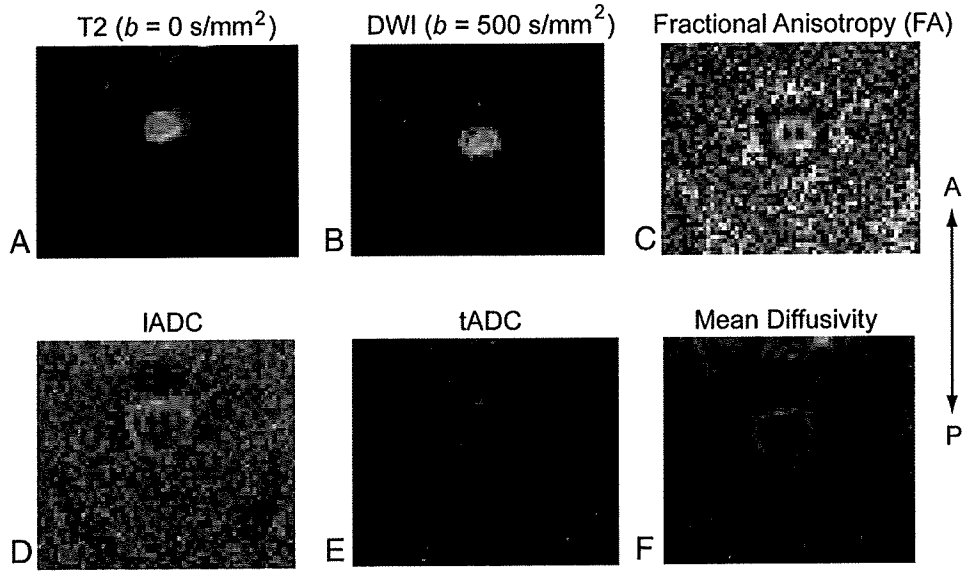

Fig. 4. Representative DTI images from an uninjured animal. (A) T_2-weighted image (b=0 s/mm^2), (B) Diffusion-weighted image (DWI, b=500 s/mm^2), (C) FA image, (D) lADC image, (E) tADC image and (F) Mean diffusivity image.

an average SNR of nearly 18 in T_2-weighted images. Fig. 4 illustrates typical T_2 (b=0 s/mm^2), diffusion-weighted (DWI, b=500 s/mm^2), FA, longitudinal apparent diffusion coefficient (lADC, largest of the eigenvalues), transverse apparent diffusion coefficient (tADC, average of two smaller eigenvalues) and mean diffusivity (average of all three eigenvalues) images in a sham-injured animal shortly after laminectomy (cat N2, 2 weeks post-surgery). Both sham-injured animals (N1 and N2) showed a consistent FA across the surgical site (Fig. 5A and B), averaging 0.59±0.04 (S.D.).

All injured animals showed a low FA at the site of injury (arrow in Fig. 5C–E) and relatively normal FA rostral and caudal from the lesion epicenter (Fig. 5C–E). To more clearly demonstrate the magnitude of this effect, average FA values from three contiguous slices at the lesion epicenter were qualitatively compared to the average FA values in the first three slices (rostral) and the last three slices (caudal) in injured animals across the different scan days (Fig. 5F). The average FA values in all slices collected for the sham-injured animals for each scan date were also plotted for comparison. As illustrated in Fig. 5F, mean FA values decreased by approximately 50% at the lesion epicenter compared to measurements in sham-injured animals.

4. Discussion

DTI has shown great promise for detecting changes in spinal cord structure through measurements of diffusion anisotropy or preferential diffusion orientation of water. Anisotropic diffusion in the central nervous system is primarily caused by barriers to diffusion such as axon cell

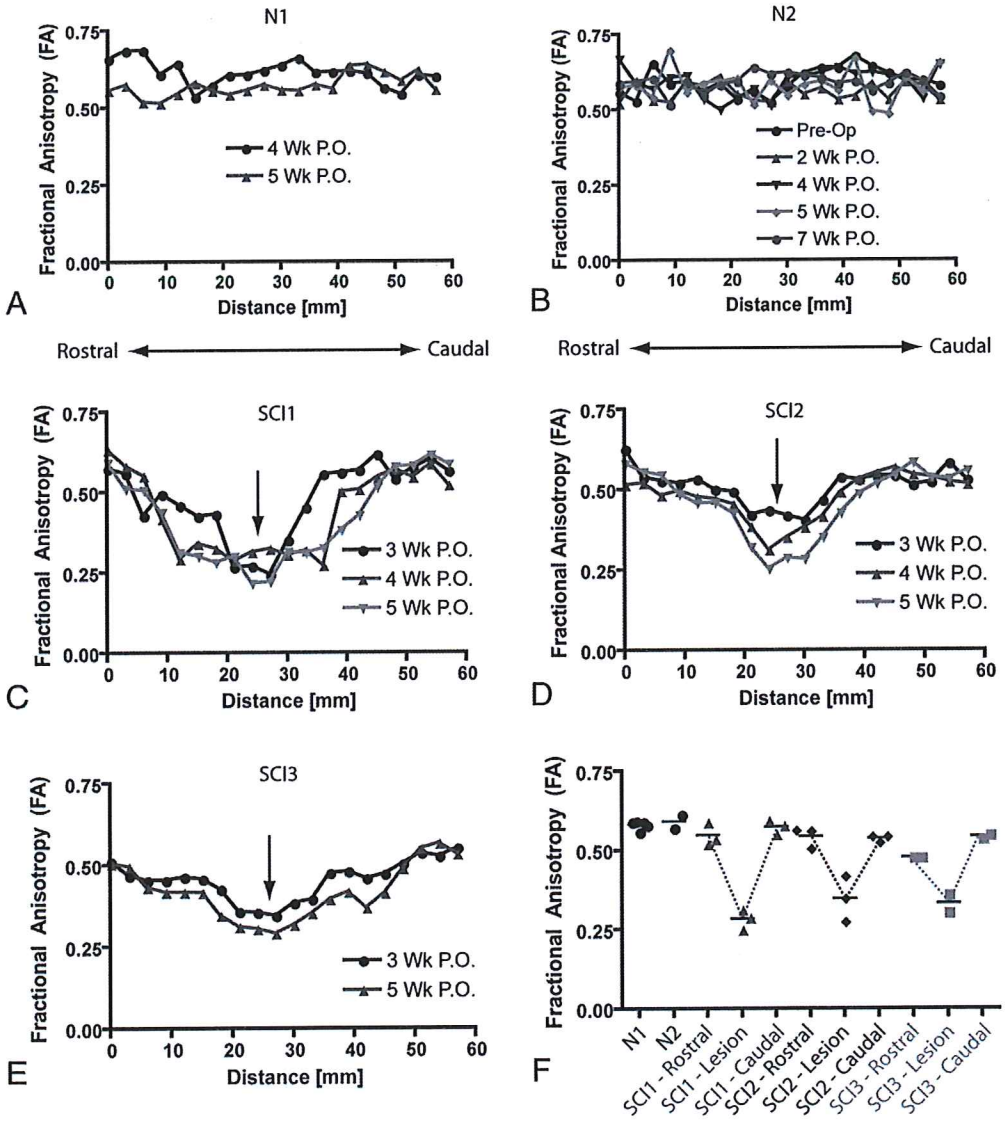

Fig. 5. FA measurements across the surgical site in cats (A) N1, (B) N2, (C) SCI1, (D) SCI2 and (E) SCI3. (F) Mean FA measurements from three contiguous slices at the lesion site and rostral/caudal to the lesion are illustrated in injured animals (SCI1, SCI2 and SCI3), along with mean FA values from uninjured animals (N1 and N2). P.O., post-operation.

membranes, and previous studies have shown that anisotropy increases with an increase in axonal fiber density, a decrease in axonal fiber diameter or a decrease in membrane permeability [16–18]. As a result, changes in diffusion can reflect underlying tissue changes associated with injury and healing processes.

Due to the recent surge in enthusiasm for applying DTI in SCI, there is an ever-growing need for cost-effective methods of acquiring DTI data on the spinal cord using clinically available MR systems with conventional gradient hardware. SNAILS-DTI is an innovative pulse sequence design that can be employed to collect high-resolution, artifact-free DTI images on clinically available MR systems. In the current study, we demonstrate the feasibility performing SNAILS-DTI on a clinical 3.0-T MR scanner to collect high spatial resolution in vivo DTI images of the cat spinal cord after spinal trauma.

4.1. Originality of the current study

The primary purpose of the current study was to demonstrate the feasibility of implementing and performing in vivo SNAILS-DTI on the injured cat spinal cord using a clinical MR system with high spatial resolution. Prior to the current study, only a single investigation examining the in vivo DTI characteristics of the cat spinal cord has been performed [11]. In this study, DTI of the cat thoracolumbar spinal cord was performed on a clinical 3.0-T MR system using a spine coil and single-shot spin-echo EPI using parallel acquisition (generalized autocalibrating partially parallel acquisition), resulting in an isotropic voxel resolution of 1.1 to 1.3 mm^3. In the current study, we were able to acquire DTI images of the cat spinal cord during free breathing with a voxel resolution of 546 μm×546 μm×3.0 mm or a voxel volume of 0.894 mm^3 (approximately 80% of the previous study voxel volume).

4.2. Limitations of the current study

The major limitation of the current study was the lack of a sufficient number of animals to perform statistical tests between sham and injured animals. Despite this limitation, qualitative observation suggests a large difference in FA between the slices within the lesion site and FA measurements in normal-appearing spinal cord tissue. This difference in FA is well documented in the literature [11,19–22] and suggests that SNAILS-DTI may be useful for quantitative comparisons in future studies.

Another limitation to the current study was the limited number of diffusion-sensitizing directions sampled to estimate the diffusion tensor. Previous investigations of the cat spinal cord have used high-angular diffusion imaging techniques, requiring more than 55 diffusion-sensitive directions [11]. In the current study, we chose to use only 25 directions, based on previous results suggesting little gain in image quality when the number of directions exceeds 25 [23] and adequate image quality in the human spinal cord with only 25 directions [19,24].

5. Conclusion

High-resolution in vivo DTI images of the cat spinal cord using clinical MR systems and conventional gradient hardware are possible with the use of a self-navigated, interleaved, variable-density spiral acquisition scheme (SNAILS-DTI). Results from the current study suggest that image quality is superior to EPI and dependent on reconstruction parameters. Results also support previous studies showing that diffusion FA is lower in injured compared to normal spinal tissue.

Acknowledgments

We would like to thank the Bryon Riesch Paralysis Foundation, the Zablocki VA Medical Center and the Department of Neurosurgery at the Medical College of Wisconsin, Milwaukee, WI, for their support. We would also like to thank Eric Paulson, Ph.D., in the Department of Radiation Oncology for his excellent work in implementing SNAILS on the clinical MR systems at our institution. We would also like to thank Christy Stadig, B.S., Carmen Clark, B.S., Angie Geiger, B.S., and Ken Allen, D.V.M., for providing the animals used in this study.

References

[1] Gudbjartsson H, Haier SE, Mulkern RV, Moocz IA, Patz S, Jolesz FA. Line scan diffusion imaging. Magn Reson Med 1996;36:509–19.
[2] Bammer R, Herneth AM, Maier SE, Butts K, Prokesch RW, Do HM, et al. Line scan diffusion imaging of the spine. Proc Intl Soc Mag Reson Med 2002:10.
[3] Young GS, Lai AP. Line scan diffusion imaging (LSDI) in clinical spine MRI: normal spectrum and correlation with anatomic MR findings. Proc Intl Soc Mag Reson Med 2002:10.
[4] Holdsworth SJ, Bammer R, Skare S. Diffusion-weighted imaging of the spine with readout-segmented (RS)-EPI. Proc Intl Soc Mag Reson Med 2009;17:634.
[5] Butts K, de Crespigny A, Pauly JM, Moseley ME. Diffusion-weighted interleaved echo-planar imaging with a pair of orthogonal navigator echoes. Magn Reson Med 1996;35(5):763–70.
[6] Wheeler-Kingshott CAM, Hickman SJ, Parker GJM, Ciccarelli O, Symms MR, Miller DH, et al. Investigating cervical spinal cord structure using axial diffusion tensor imaging. Neuroimage 2002;16 (1):93–102.
[7] Fellner C, Menzel C, Fellner FA, Ginthör C, Zorger N, Jung EM, et al. BLADE in sagittal T2-weighted imaging of the cervical spine: reduction of artifacts and value for clinical application. Proc Intl Soc Mag Reson Med 2009;17:1308.
[8] Liu C, Bammer R, Kim D, Moseley ME. Self-navigated interleaved spiral (SNAILS): application to high resolution diffusion tensor imaging. Magn Reson Med 2004;52(6):1388–96.
[9] Meyer CH, Hu BS, Nishimura DG, Macovski A. Fast spiral coronary artery imaging. Magn Reson Med 1992;28(2):202–13.
[10] Kim D, Adalsteinsson E, Spielman DM. Simple analytic variable density spiral design. Magn Reson Med 2003;50(1):214–9.

[11] Cohen-Adad J, Benali H, Hoge RD, Rossignol S. In vivo DTI of the healthy and injured cat spinal cord at high spatial and angular resolution. Neuroimage 2008;40(2):685–97.
[12] Glover GH. Simple analytic spiral k-space algorithm. Magn Reson Med 1999;42(2):412–5.
[13] Crowe MJ, Sun ZP, Battocletti JH, Macias MY, Pintar FA, Maiman DJ. Exposure to pulsed magnetic fields enhances motor recovery in cats after spinal cord injury. Spine 2003;28:2660–6.
[14] Reese TG, Heid O, Weisskoff RM, Wedeen VJ. Reduction of eddy-current-induced distortion in diffusion MRI using a twice-refocused spin echo. Magn Reson Med 2003;49(1):177–82.
[15] Kaufman L, Kramer DM, Crooks LE, Ortendahl DA. Measuring signal-to-noise ratios in MR imaging. Radiology 1989;173(1): 265–7.
[16] Schwartz ED, Cooper ET, Fan Y, Jawad AF, Chin CL, Nissanov J, et al. MRI diffusion coefficients in spinal cord correlate with axon morphometry. Neuroreport 2005;16(1):73–6.
[17] Ford JC, Hackney DB. Numerical model for calculations of apparent diffusion coefficient (ADC) in permeable cylinders — comparison with measured ADC in spinal cord white matter. Magn Reson Med 1997;37(3):387–94.
[18] Ford JC, Hackney DB, Alsop DC, Jara H, Joseph PM, Hand CM, et al. MRI characterization of diffusion coefficients in a rat spinal cord injury model. Magn Reson Med 1994;31(5):488–94.
[19] Ellingson BM, Ulmer JL, Kurpad SN, Schmit BD. MR imaging in chronic spinal cord injury. AJNR Am J Neuroradiol 2008;29(10): 1976–82.
[20] Ellingson BM, Kurpad SN, Schmit BD. Ex vivo diffusion tensor imaging and quantitative tractography of the rat spinal cord during long-term recovery from moderate spinal contusion. J Magn Reson Imaging 2008;28(5):1068–79.
[21] Shanmuganathan K, Gullapalli RP, Zhuo J, Mirvis SE. Diffusion tensor MR imaging in cervical spine trauma. AJNR Am J Neuroradiol 2008;29(4):655–9.
[22] Deo AA, Grill RJ, Hasan KM, Narayana PA. In vivo serial diffusion tensor imaging of experimental spinal cord injury. J Neurosci Res 2006;83(5):801–10.
[23] Poonawalla AH, Zhou XJ. Analytical error propagation in diffusion anisotropy calculations. J Magn Reson Imaging 2004;19:489–98.
[24] Ellingson BM, Ulmer JL, Kurpad SN, Schmit BD. Diffusion tensor MR imaging of the neurologically intact human spinal cord. AJNR Am J Neuroradiol 2008;29(7):1279–84.